

A Low-Cost and Low-Power CMOS Receiver Front-End for MB-OFDM Ultra-Wideband Systems

Mahim Ranjan, *Member, IEEE*, and Lawrence E. Larson, *Fellow, IEEE*

Abstract—This paper presents an RF receiver front-end for MB-OFDM-based ultra-wideband (UWB) systems. The receiver occupies only 0.35 mm² in a 0.18 μm CMOS process and consists of a low-noise amplifier, downconverter and a bandpass filter. There are no on-chip inductors and the receiver requires no off-chip matching components. The measured receiver gain is 21 dB, noise figure is less than 6.6 dB, input IIP₃ is −5.6 dBm, and the receiver consumes 19.5 mA from a 2.3 V supply. The receiver covers all the MB-OFDM bands from 3.1 to 8 GHz.

Index Terms—CMOS, distortion, OFDM, receiver, ultra wideband, UWB.

I. INTRODUCTION

ULTRA-WIDEBAND (UWB) multi-band orthogonal frequency-division multiplexing (MB-OFDM) systems have been proposed as an emerging solution to wireless communication applications requiring high data rates (up to 480 Mb/s) over short distances. In one proposed version [1], the carrier, with a bandwidth of 528 MHz, can hop to one of 14 channels (2904 + 528*n*, *n* = 1, 2, . . . , 14), divided into four groups of three channels and one group of two channels. This representative time-frequency interleaving for a Group 1-only system is depicted in Fig. 1. Design of a receiver for such a system presents many challenges due to the wide bandwidth of the RF front-end. However, to assure the widest possible adoption, RF portions of these systems should consume little DC power and die area, and be implemented in a standard CMOS process. These last requirements argue against the use of on-chip inductors wherever possible.

Since the UWB front-end intrinsically possesses a wide bandwidth, it is open to reception of undesired narrowband signals such as 802.11 a/b/g and the recently proposed WiMAX [2] systems, as shown in Fig. 2. Although OFDM systems are less susceptible to relatively narrowband jammers, nonlinearities in the receiver can result in jammer cross-modulation with wideband input signals, resulting in reduced signal-to-noise ratio (SNR) and a degradation in system performance [3]. In addition, received wideband signals (from other UWB transmitters) can intermodulate and the resulting products can land in a desired

Manuscript received May 25, 2006; revised August 24, 2006. This work was supported by Qualcomm, the Center for Wireless Communication at UC San Diego, and a UC Discovery Grant.

M. Ranjan was with the University of California at San Diego, La Jolla, CA 92093-0407 USA. He is now with Qualcomm Inc, San Diego, CA 92121 USA (e-mail: mranjan@qualcomm.com; mahimranjan@yahoo.com).

L. E. Larson is with the Department of Electrical and Computer Engineering, University of California at San Diego, La Jolla, CA 92093-0407 USA (e-mail: larson@ece.ucsd.edu).

Digital Object Identifier 10.1109/JSSC.2006.891725

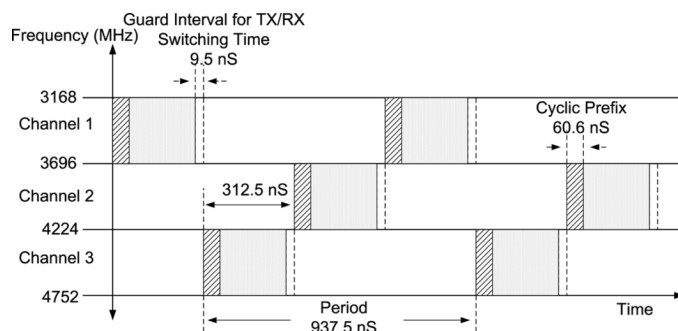


Fig. 1. Representative time-frequency interleaving pattern of a Group 1 MB-OFDM signal [1].

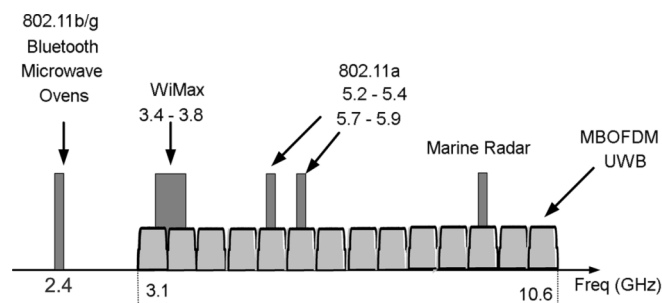


Fig. 2. Representative spectrum at an MB-OFDM receiver antenna.

channel. Since the system is inherently wideband, harmonic distortion of a single unwanted UWB transmitter can also produce in-band distortion products and reduce the SNR. For the system to successfully operate in such a hostile environment, the linearity specifications of the receiver need to include these distortion effects.

This paper describes a UWB heterodyne receiver front-end that is designed to minimize the effects of wideband jammers from a variety of undesired sources [4]. In addition, the receiver is designed to minimize silicon area, so on-chip inductors are not employed. The receiver architecture is presented in Section II. Specifications for the receiver are derived in Section III. Detailed block design is presented in Sections IV–VI. Layout and packaging of the chip is discussed in Section VII. Measured results are presented in Section VIII, followed by a conclusion in Section IX.

II. RECEIVER ARCHITECTURE

When it comes to designing a low-power and low-cost receiver, the traditional choice is a direct conversion architecture. However, a direct conversion UWB receiver, while attractive for power consumption and simplicity of its local oscillator (LO)

scheme [5], [6], has a well-known problem of time-varying DC offset and sensitivity to narrowband jammers. A DC offset at the output of the receiver can degrade the SNR of the digitized baseband signal. In addition, it can introduce second-order distortion in the baseband signal, which further degrades the SNR.

Since the LO can vary from 3.5 to 8 GHz, the DC offset present at the mixer output can vary significantly with every frequency hop. Since the frame can be as short as 312.5 ns, as shown in Fig. 1, the DC offset calibration has to settle within that time interval. Designing an offset calibration loop that settles this quickly is a significant challenge. A DC blocking capacitor at the receiver baseband output can reduce the DC offset, but does not reduce second-order distortion in the mixer. In addition, since the received signal strength will change with every frequency hop, the DC blocking capacitor will introduce a significant settling time, of the order of microseconds.

On the other hand, a heterodyne receiver is less sensitive to the impairments of a direct conversion architecture, but poses several challenges of its own in terms of cost and current consumption. A heterodyne receiver usually requires more components in the receiver chain, which can result in a larger die area and higher current consumption. Two of the main drawbacks with a heterodyne receiver are the need for image rejection and an IF bandpass filter. Image rejection is usually achieved with an image reject mixer and/or a highly selective image reject filter. An image reject mixer for a UWB system is particularly challenging, since the mixer will need an accurate quadrature local oscillator to be generated over a very wide fractional bandwidth. In addition, the current consumption of an image reject mixer is significantly larger than a single mixer.

A bandpass filter is required at the IF output to mitigate the linearity requirements on the following IF downconverter chain. The filter needs to suppress the adjacent channels present in a multiple-piconet UWB system. On-chip passive bandpass filters require high-Q inductors, which can add significant die area and force the use of a thick top metal, which will add to the total cost of the die. Active filters, on the other hand, can be very power hungry and can also cause a significant increase in the noise figure and distortion of the system [7]. These are the main challenges that need to be overcome for a viable heterodyne receiver.

To avoid the classical heterodyne receiver image rejection problem, the frequency plan was designed for an IF of 2.64 GHz, so that all the images fall below 2.4 GHz. Therefore, an external bandpass filter with a lower cut-off frequency of 3 GHz, which is standard in UWB receiver designs, suppresses all the images, as shown in Fig. 3. In addition, the tunable LNA provides further image rejection. The resulting image rejection is sufficient to eliminate the need for an image reject mixer. However, this choice of the IF limits the image rejection to Band Groups 1, 2, and 3 only. For higher band groups (beyond 8 GHz), with an IF of 2.64 GHz, the images will be above 3.1 GHz in frequency and will not be attenuated by the external bandpass filter (BPF).

III. RECEIVER SPECIFICATIONS

A. Receiver Linearity

1) *Receiver IIP₃*: Although UWB systems have not been widely deployed, it is recognized that the interference environ-

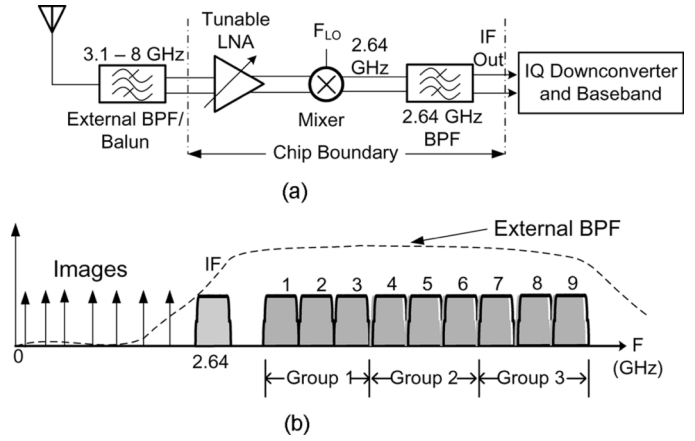


Fig. 3. (a) Proposed receiver architecture. (b) Receiver frequency plan. All the images are outside the desired band.

ment for these devices is a challenge. Potential in-band interferers include WiMAX and WiFi devices, as well as airport and marine radars [8]. For the receiver to maintain adequate link margin and sensitivity, careful consideration needs to be given to cross-modulation distortion [3], [9].

In a typical cross-modulation scenario, the UWB system might receive a narrowband jammer at -30 dBm (a WiMAX signal for one example), along with a wideband jammer from another transmitting UWB system, which could be located as close as 0.1 m from the receiver. The average transmitted power of a UWB transmitter is -10.3 dBm [1]. At 0.1 m, this power would drop to roughly -34.5 dBm for a Mode 1 system. The cross-modulation product of a narrowband jammer with an MB-OFDM transmitter is given by [3]

$$PSD_{XMOD}(\omega) = \frac{c_3^2}{2} (A_j A_{tx}^2)^2 T_s \sum_{m=-\frac{N_s}{2}}^{\frac{N_s}{2}} \sum_{n=-\frac{N_s}{2}}^{\frac{N_s}{2}} \text{sinc}^2((\omega + (\omega_j + \Delta\omega(m-n)) T_s)) + \text{sinc}^2((\omega - (\omega_j + \Delta\omega(m-n)) T_s)) \quad (1)$$

where ω_j is the frequency of the narrowband jammer and ω_{tx} is the center frequency of the second unwanted MB-OFDM transmitter. A_j is the amplitude of the narrowband jammer, A_{tx} is the peak amplitude per carrier of the second unwanted MB-OFDM transmitter, and c_3 is the third-order distortion coefficient of the receiver. N_s is the number of subcarriers in the MB-OFDM system and T_s is the symbol duration. A_{tx} can be related to the total RF MB-OFDM input power of P_{in} , normalized to 1 Ω , as [3]

$$P_{in} = \frac{N_s A_{TX}^2}{\pi} \quad (2)$$

The effect of receiver IIP₃ on the SNR due to this cross-modulation distortion can be computed by integrating (1) over the bandwidth of one MB-OFDM receive band.

For example, assuming a noise figure of 6 dB and an overall gain of 15 dB for the LNA/downconverter, the output noise power at the desired channel of 3.5 GHz is -65.84 dBm. With a narrowband jammer of -40 dBm at 3 GHz and a wideband

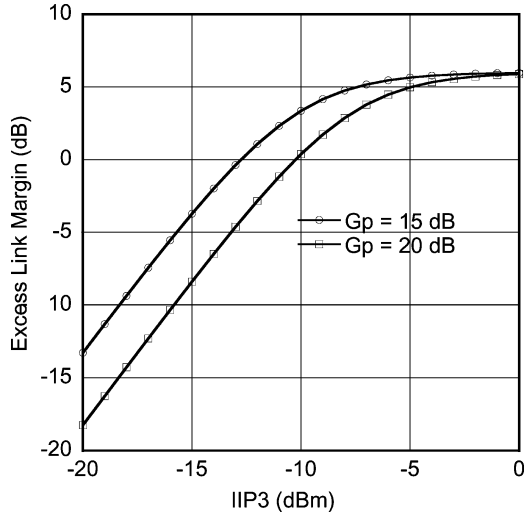


Fig. 4. Receiver link margin for the case of a narrowband jammer at -40 dBm and a wideband jammer at -34.5 dBm.

jammer of -34.5 dBm at 4.4 GHz [3], integrating (1) from 3150 to 3500 MHz, corresponds to a total cross-modulation power at the mixer output of -66.6 dBm. This cross-modulation effectively increases the noise figure of the receiver by 2.6 dB.

Fig. 4 plots the link margin of the receiver as a function of receiver IIP_3 for a receiver gain of 15 dB and 20 dB using (1), when the narrowband jammer power is -40 dBm and wideband jammer power is -34.5 dBm. It can be seen from the plots that a receiver IIP_3 of -5 dBm results in a link margin degradation of less than 1 dB. The receiver was therefore designed for an IIP_3 of -5 dBm.

2) *Receiver IIP_2* : Receiver IIP_2 is usually not very important for heterodyne receiver front ends. However, in an MB-OFDM system, since the second-order intermodulation product (IM_2) of two undesired transmitters may land in a desired channel, close attention needs to be given to receiver IIP_2 specification. For example, the IM_2 product of 3432 MHz (Band 1) and 3960 MHz (Band 2) would be at 7392 MHz, which will reduce the SNR of a desired signal in either Band 8 or Band 9 of an MB-OFDM system, since the IM_2 product is spread to twice the bandwidth of the original signal. This situation is depicted in Fig. 5.

The power spectral density (PSD) of this IM_2 product can be computed using [3]

$$PSD_{IM_2}(\omega) = c_2^2 A_{tx1}^2 A_{tx2}^2 T_s \sum_{m=-\frac{N_s}{2}}^{\frac{N_s}{2}} \sum_{n=-\frac{N_s}{2}}^{\frac{N_s}{2}} \left\{ \text{sinc}^2((\omega + (\omega_{tx1} + \omega_{tx2} + \Delta\omega(m+n))T_s)) \right. \\ \left. + \text{sinc}^2((\omega - (\omega_{tx1} + \omega_{tx2} + \Delta\omega(m+n))T_s)) \right\}. \quad (3)$$

The effect of IM_2 distortion in the receiver on the total link margin for the situation depicted in Fig. 5 is shown in Fig. 6. The receiver gain is assumed to be 20 dB and the noise figure is 6 dB. It can be seen that the effect of IM_2 distortion is negligible if the receiver IIP_2 is greater than 20 dBm. Therefore, the receiver shall be designed for an IIP_2 of 20 dBm.

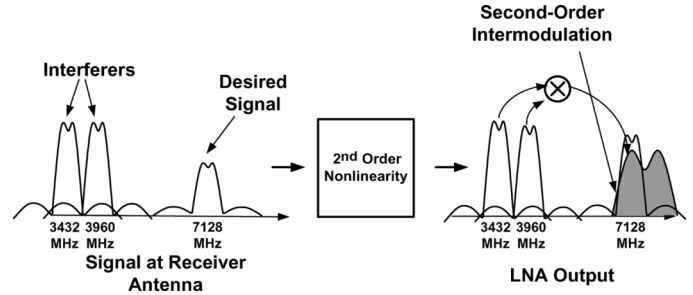


Fig. 5. Second-order intermodulation distortion in a receiver front-end.

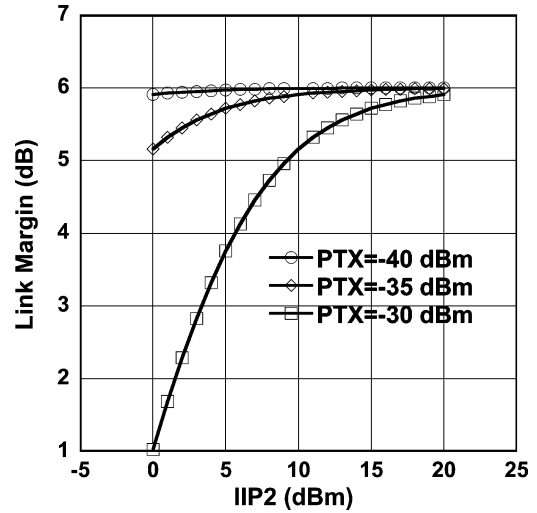


Fig. 6. Effect to receiver IIP_2 on total link margin. Receiver gain is 20 dB and noise figure is 6 dB.

B. Receiver Gain and Noise Figure

To reduce the impact of the IF downconverter noise figure on the total receiver noise figure, it is advantageous to provide as large a gain in the front-end as possible. However, this can lead to two complications. First, since the LNA is very wideband, providing a large gain will prove to be expensive in terms of power consumption. Additionally, a high gain in the receiver front-end will increase the linearity requirement of the RF mixer and the IF downconverter chain, which could lead to even higher power consumption.

For example, consider the situation of three nearby MB-OFDM transmitters, transmitting at their maximum power of -10.3 dBm. At 0.1 m, the front-end receives three MB-OFDM signals with a total maximum received power of -29.7 dBm. To avoid gain compression in the front-end, the input referred 1-dB compression point has to be greater than -29.7 dBm. Adding another 10 dB of margin, the receiver input referred 1-dB compression point should be -19.7 dBm. Representing the receiver nonlinearity as a third-order power series and using the well-known approximation

$$IIP_3 \approx P1 \text{ dB} + 10 \quad (4)$$

the required LNA IIP_3 will be -9.7 dBm.

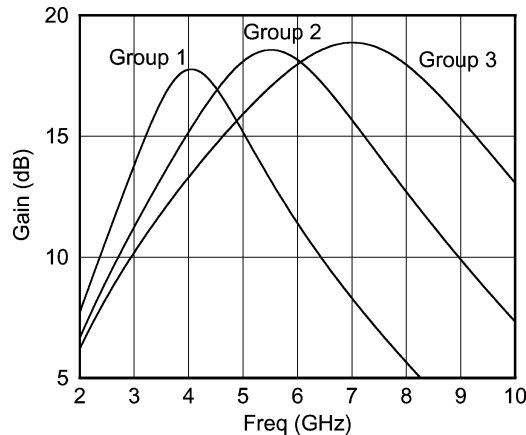


Fig. 10. Simulated frequency response of tuned output LNA.

the three highest bands (6.3–8 GHz). When the received signal is in the lower bands of Group 2 or Group 1, extra shunt capacitance is switched in, by setting bits b_0 and b_1 “high” successively, to dynamically maximize the gain of the LNA at 5.5 GHz and 4 GHz.

This scheme allows for load tuning of the LNA without using any on-chip inductors. However, it does have a drawback in sensitivity to bondwire length. The bondwire inductance for this package at the LNA input and LNA output was approximate 1.2 nH. In a typical bonding process, the variation in bondwire length is usually $\pm 10\%$. Additionally, the tank capacitance can vary by $\pm 20\%$ due to variation in device output capacitance and variation in the shunt tuning capacitors. This variation would result in a center frequency variation of $\pm 15\%$. However, the simulation results of Fig. 10 show that this will result in at most a 1 dB drop in gain at band edges, which is not significant. The reduced susceptibility to variations in bondwire length and on-chip capacitance can be attributed to the low Q of the LNA load tank.

A differential design is employed to reduce second-order distortion, which is a serious concern for wideband systems since the second-order intermodulation product of two unwanted jamming transmitters can appear in the band of interest. Also, if a single-ended amplifier were employed, the downbond inductance of the package would act as source degeneration for the amplifier. This degeneration would be frequency dependent and the amplifier gain would be a strong function of the input frequency.

Broadband input matching of the amplifier was achieved by a shunt RC feedback network, as shown in Fig. 9. Although this provides for a good wideband input match, it degrades the noise figure of the LNA. The simulated worst case noise figure of this LNA was 4.5 dB, which is higher than that reported in [11]–[13]. However, this noise figure is adequate to maintain a 6.0 dB noise figure for the entire front-end. Even with a worst case LNA noise figure of 4.5 dB and gain of 15 dB, the required RF mixer noise figure is 16 dB or less, to achieve a receiver noise figure of 6 dB.

The LNA consumes 11 mA from a 2.3 V supply, and simulated gain was between 15–18.5 dB. The simulated IIP_3 was -4 dBm and the worst case input return loss was -7 dB. The

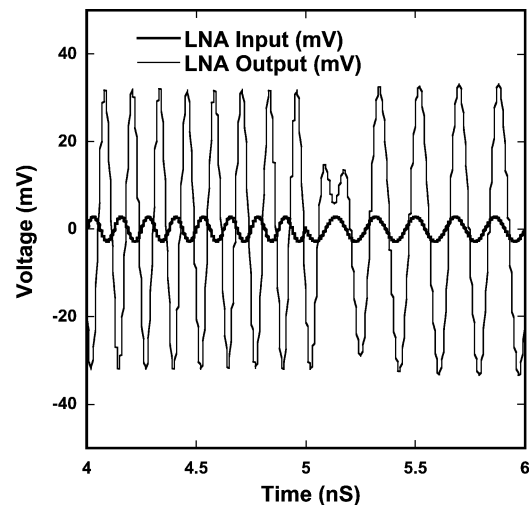


Fig. 11. Simulated switching time of the LNA, when tuning from Band 8 to Band 5. Switching time is less than 1 ns.

performance and power consumption of this LNA is comparable to that reported in [11]–[13], but this LNA has a significantly smaller die area, since no on-chip inductors are needed. The simulated band switching time for the LNA is shown in Fig. 11, and is less than 1 ns.

Additionally, this LNA provides rejection of undesired jammers and images. For example, when the receiver is tuned to Group 3, from the simulated LNA frequency response in Fig. 10, it can be seen that the LNA rejects the signal from any transmitter transmitting in Group 1 or Group 2 by at least 4 dB. The LNA frequency response also provides for a minimum of 8 dB rejection of 802.11b/g and Bluetooth jammers transmitting in the 2.4 GHz unlicensed band.

For the frequency plan described in Section II, all the images are below 2.64 GHz. The received signal and its image are closest when the received signal is in Band 1 at 3432 MHz. The image is then at 1848 MHz. It can be seen from Fig. 10 that the LNA provides approximately 10 dB of image rejection in this case. Therefore, significant image rejection has been achieved with this LNA design, reducing the need for an image reject mixer or a front end image reject filter.

V. RF DOWNCONVERTING MIXER

The downconverter (Fig. 12) is a wideband, double balanced Gilbert Cell based mixer. The LNA provides for a minimum of 10 dB of image rejection and further image suppression is obtained by the external bandpass filter before the LNA. Therefore, the mixer does not need to provide any additional image rejection. Resistive loading and degeneration was employed in the mixer for wideband performance.

The simulated gain for the mixer was 0 dB and its simulated noise figure was 13 dB. The mixer consumes 8.5 mA from a 2.3 V supply.

VI. IF BANDPASS FILTER

Since there might be multiple MB-OFDM transmitters operating in the vicinity, it is necessary to provide for some on-chip

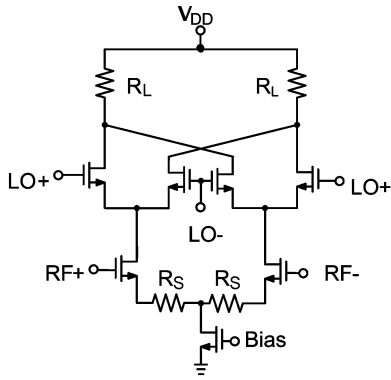


Fig. 12. Active double-balanced mixer schematic.

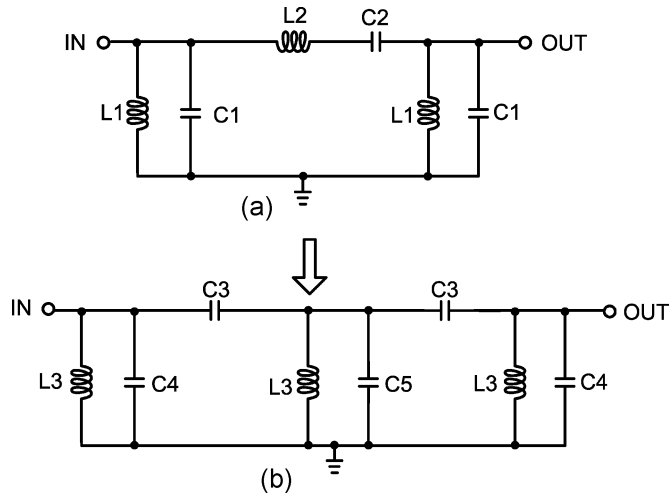


Fig. 13. Bandpass filter design. (a) Chebyshev bandpass prototype. (b) Bandpass filter after impedance inversion.

IF channel selection to ease linearity requirements on the remainder of the receive chain and eliminate the need for an external IF filter. Unfortunately, active filters have well known dynamic range and power limitations, and an on-chip LC filter would require high-Q inductors and significant die area. The goal of this design is to keep the area as small as possible, while maintaining adequate performance.

A standard single-ended bandpass Chebyshev filter (Fig. 13) would require three inductors, one of which would be very large. Usually, the ratio of the inductor in the shunt resonator to the inductor in the series resonator is of the order of the square of the fractional bandwidth of the filter [15]. For our purposes, the fractional bandwidth is approximately 1/5. Even if the shunt inductors were as small as 1 nH, the series inductor would have to be approximately 25 nH. Filter loss and adjacent channel rejection are directly related to the Q of these inductors. If such a filter were to be designed on-chip, it would require a very large die area and thick top metal for high Q inductors.

An impedance inversion transformation [15] was applied to a standard single-ended third-order passive bandpass Chebyshev filter, resulting in a “top-C” coupled structure, with fixed equal-valued shunt grounded inductors, as shown in Fig. 13. It is important to note that this impedance transformation is valid for only one frequency, so the filter rejection is limited compared

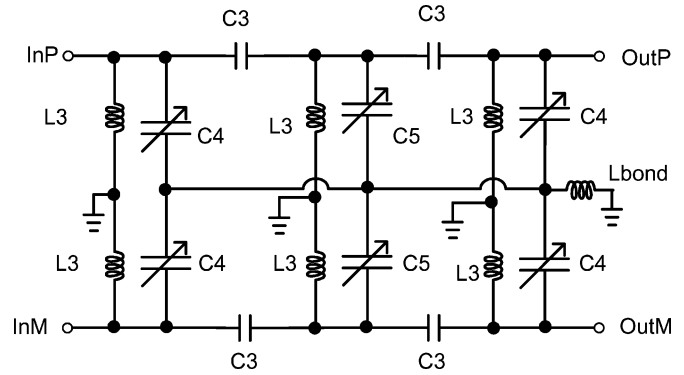


Fig. 14. Final differential bandpass filter employing only equal-valued grounded bondwire inductance.

to the third-order prototype filter. All the inductors in this filter are grounded and can therefore be replaced with downbonds, which have a very high Q. The resulting filter in its differential form is shown in Fig. 14. The downbond inductance for our package was determined to be 0.8 nH and the capacitor values were chosen appropriately.

The filter was designed for an IF center frequency of 2.64 GHz and a bandwidth of 528 MHz. Since the on-chip capacitance can vary by $\pm 20\%$ and the bondwire inductance can vary by approximately $\pm 10\%$, it is important to provide some mechanism for tuning the bandpass filter. To this end, the shunt capacitors in the bandpass filters were replaced by MOS varactors. The measured tuning range was ± 300 MHz, which is enough to accommodate the capacitance and bondwire inductance variation. The nonlinear C–V characteristic of the varactor diode has relatively little effect on the circuit performance, since the voltage level at the input to the filter is relatively small. A varactor diode provides continuous tuning of the frequency range of the filter, although in practice digital control of a MIM capacitor array would function equally well. Various filter tuning techniques, such as those described in [16] and [17] can be used for frequency tuning of this filter.

A potential problem with this filter is the possibility of noise coupling onto the bond-wires. But since the receiver has almost 20 dB of gain before the filter, this is not a significant issue.

A. Impact of IF Bandpass Filter

The filter is especially important in a high interference scenario, since it eases both the gain compression and the intermodulation specification of the IF downconverter. If an off-chip filter were to be employed, it would increase the cost of the system since high-frequency off-chip bandpass filters are expensive, extra pins would be required for the signal to be routed off-chip and the off-chip filter can occupy significant board area.

1) *IF Downconverter Gain Compression:* In the high interference scenario of three adjacent MB-OFDM transmitters, transmitting at their maximum power of -10.3 dBm, the signal at the receiver antenna is -34.5 dBm from each of the transmitters, for a total input power of -29.7 dBm. With a 20 dB gain in the RF chain, this results in a receiver output of -9.7 dBm.

However, an IF bandpass filter with an adjacent channel rejection of 8 dB, suppresses the two unwanted sidebands by 8 dB.

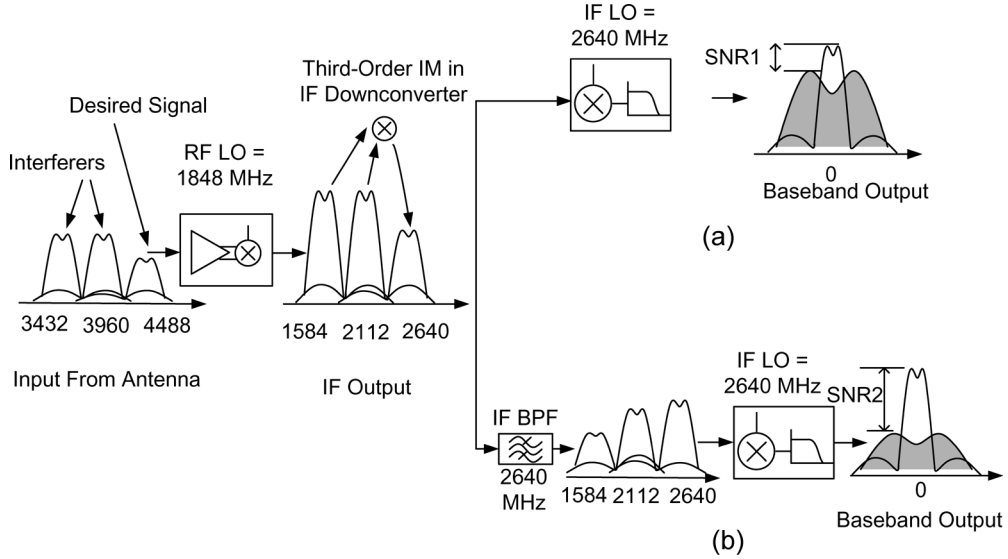


Fig. 15. Third-order IM distortion in the IF downconverter. (a) Without an IF channel select filter. (b) With an IF channel select filter.

The power at the IF downconverter input will be -14.5 dBm in the desired channel, and -22.5 dBm in each of the two adjacent channels, resulting in an output power of -13.3 dBm. The IF bandpass filter, therefore, eases the gain compression specification of the IF downconverter by 3.6 dB.

2) *IF Downconverter Intermodulation Distortion*: The BPF also reduces the intermodulation distortion requirement on the IF downconverter. In a typical intermodulation distortion scenario, adjacent channels present at the IF input can downconvert to baseband in the presence of third-order nonlinearity in the IF downconverter, resulting in reduced baseband SNR.

As shown in Fig. 15, a channel select filter at the RF downconverter output can improve the SNR at the baseband output. This implies that, for a given baseband output SNR, a channel select filter reduces the third-order intermodulation specification of the IF downconverter.

To calculate the intermodulation output at baseband, we can use [3]

$$PSD_{IM3}(\omega) = \frac{9}{4} c_3^2 A_{tx1}^4 A_{tx2}^2 T_s \sum_{k=-\frac{N_s}{2}}^{\frac{N_s}{2}} \sum_{m=-\frac{N_s}{2}}^{\frac{N_s}{2}} \sum_{n=-\frac{N_s}{2}}^{\frac{N_s}{2}} \left\{ \text{sinc}^2((\omega + (2\omega_{tx1} - \omega_{tx2} + \Delta\omega(m+n+k))T_s) \right. \\ \left. + \text{sinc}^2((\omega - (2\omega_{tx1} - \omega_{tx2} + \Delta\omega(m+n+k))T_s) \right\} \quad (5)$$

where A_{tx1} and A_{tx2} are the peak amplitudes per carrier of the two undesired MB-OFDM signals and can be related to the corresponding RF input power using (2), ω_{tx1} and ω_{tx2} are the angular frequencies. Equation (5) can be integrated over the bandwidth of one MB-OFDM channel to obtain the total output noise power due to intermodulation.

In the situation described in Fig. 15, the degradation in baseband SNR due to third-order distortion in the IF downconverter can be calculated by adding the intermodulation distortion power from (5) to the total output noise at baseband. From [1], the required baseband SNR is 6.5 dB (required E_b/N_0 of 4 dB plus an implementation loss of 2.5 dB). Assuming an IF downconverter gain of 60 dB and noise figure of 10 dB, using (5), it

can be shown that the IF downconverter IIP_3 has to be 7.5 dBm to maintain a 6.5 dB SNR in the presence of two jamming signals at -14.5 dBm. However, with the channel select filter, which provides an 8 dB rejection of the closest channel and a 12 dB rejection of the second adjacent channel, to maintain the same SNR at baseband, the required IF downconverter IIP_3 is only -8 dBm. This channel select filter, therefore, relaxes the IIP_3 distortion specification of the IF downconverter by approximately 15 dB.

This reduction in required IIP_3 of the IF downconverter can also be estimated in the following way.

The filter attenuates the closest adjacent channel by 8 dB and the second adjacent channel by 15 dB. This implies that A_{tx1} in (5) should be replaced by $A_{tx1}/2.5$ and A_{tx2} in (5) should be replaced by $A_{tx2}/4$. Since the PSD of the IM_2 product is proportional to the A_{tx}^2 , this gives an overall reduction in the PSD of the IM_3 product by approximately 14 dB. Therefore, c_3^2 , which represents the third-order distortion product in the receiver, can be increased by 14 dB to maintain the same distortion component.

VII. CHIP LAYOUT AND PACKAGING

Since this design relies on accurate modeling, careful positioning of individual blocks and bondwires is essential. Fig. 16 shows a block diagram of the chip and the bondwires.

Inductance coupling between bondwires is an issue since it can result in spurious tones and even result in instability in the circuit. Simulations determined that coupling between the down-bonds of the bandpass filter created undesired poles and zeroes and significantly affected the performance of the filter. In addition, since it is difficult to accurately estimate the coupling coefficient between the bondwires, it is hard to predict the resulting performance of the filter. Electromagnetic simulations (using Momentum EM simulator) demonstrated that the mutual coupling coefficient between adjacent bondwires was 0.4, and that the mutual coupling coefficient between bond wires separated by at least one other bondwire was less than 0.1.

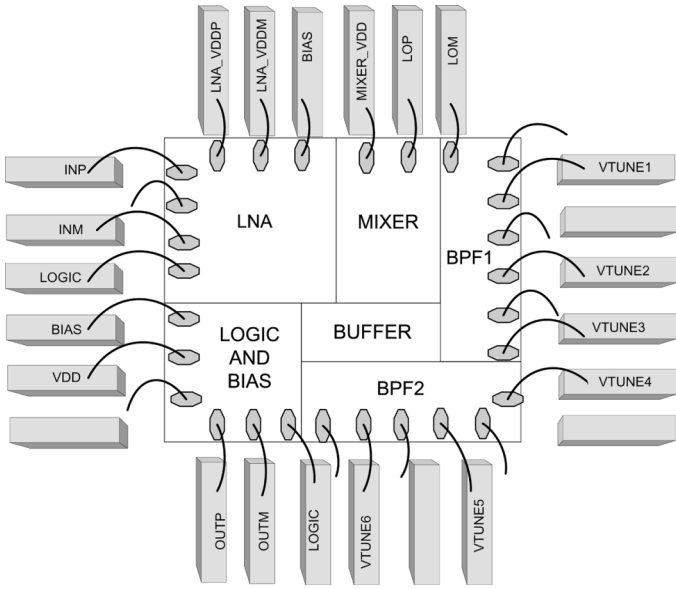


Fig. 16. Layout of UWB receiver.

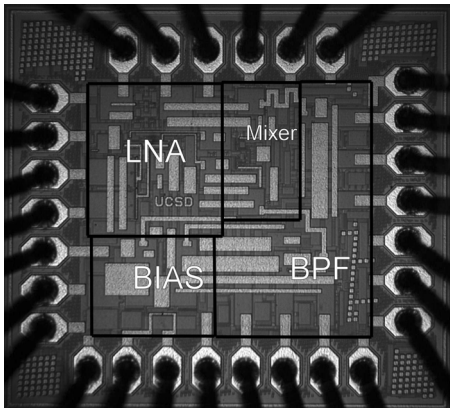


Fig. 17. UWB receiver micrograph. The active area is 0.35 mm².

It was determined, in simulations, that a mutual coupling coefficient of less than 0.1 had a negligible impact on the performance of the BPF. Therefore, all the downbands in the filter are separated by at least one bondwire. In addition, the two differential halves of the bandpass filter were placed on perpendicular edges of the chip to reduce coupling between the two sides. Similarly, the LNA input and load tank bondwire pins were placed on perpendicular edges of the chip to reduce the coupling that would lead to potential instability. Fig. 16 shows the layout of the chip and positioning of bondwires and Fig. 17 is a micrograph of the chip.

The chip was fabricated in the Jazz Semiconductor 0.18 μm RF CMOS process and was packaged in a 24 pin MLF package.

VIII. MEASURED RESULTS

To measure the receiver performance, the LO and input ports were driven by a coaxial balun. The measured gain of the receiver in each of the MB-OFDM Bands is shown in Fig. 18. The gain varies from 15 dB in Band 1 (3.5 GHz) to 21 dB in Band 8 (7.1 GHz). This gain variation is expected due to the

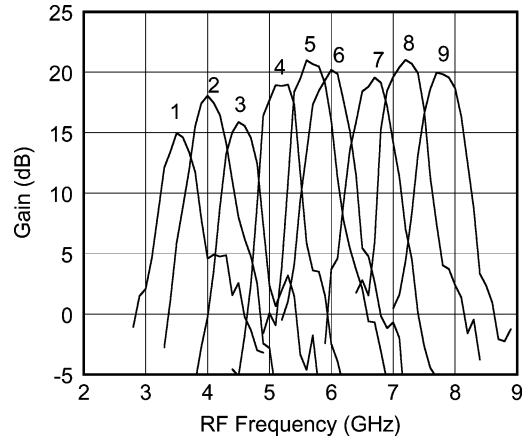


Fig. 18. Measured receiver gain in UWB bands 1-9.

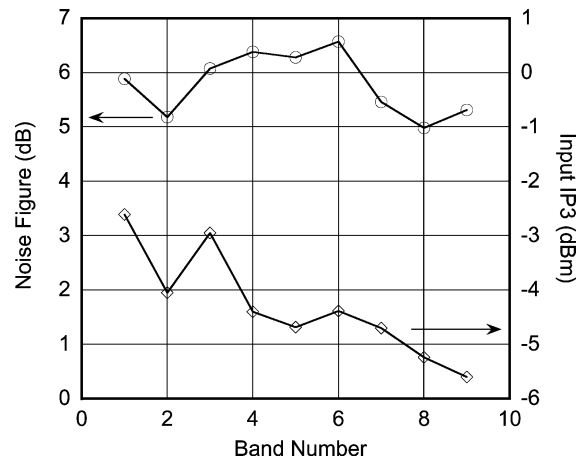


Fig. 19. Measured receiver noise figure and IIP₃.

TABLE I
RECEIVER POWER CONSUMPTION

LNA	11 mA
Mixer	8.5 mA
Power Supply	2.3V

loss in the switches of the shunt capacitors C1/C2 in Fig. 9. Although the gain varies by 6 dB between the bands, this is not a significant issue since the received signal strength will vary significantly over frequency. The receiver gain drops by roughly 2 dB at each of the band edges, but this has a small effect, since the ten carriers at the band edge are guard carriers [1].

The measured receiver IIP₃ and noise figure are plotted in Fig. 19. The noise figure varies between 5 and 6.6 dB. This is due to both the variation in LNA gain and the variation in image rejection from the LNA (Fig. 21). The measured IIP₃ is between -5.6 dBm and -2.6 dBm, which is sufficient for the receiver to perform adequately in the cross-modulation scenario discussed in Section III-A.

Second-order intermodulation distortion in the receiver is important, since the IM₂ product of two undesired transmitters may land in a desired channel. IIP₂ of the receiver was measured by injecting a single tone in Band 1 and measuring the second harmonic at the output, while tuning the receiver to Band 7.

TABLE II
SUMMARY OF MEASURED RECEIVER PERFORMANCE

Band no	Freq.	Gain	NF	IIP_3	BPF Rej.	Im. Rej.
	MHz	dB	dB	dBm	dB	dB
1	3432	15	5.8	-2.6	10.4	6.8
2	3960	18	5.2	-4	10	16.2
3	4488	15.9	6	-3	13.5	25.4
4	5016	18.9	6.38	-4.4	13	36
5	5544	21	6.28	-4.7	9.8	37
6	6072	20.2	6.57	-4.4	7.9	36
7	6600	20.3	5.46	-4.7	7.5	27
8	7128	21	5	-5.2	9.1	22
9	7656	20	5.3	-5.6	7.5	19

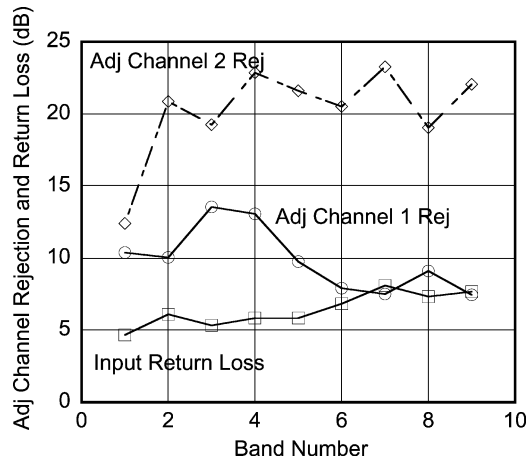


Fig. 20. Measured BPF adjacent channel rejection and input return loss.

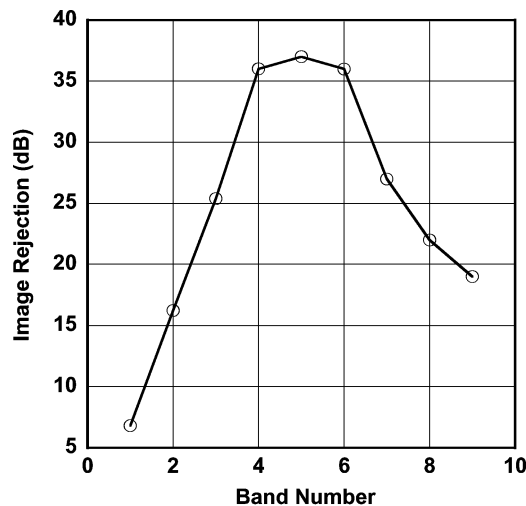


Fig. 21. Measured receiver image rejection.

The measured IIP_2 of the receiver was 33 dBm, which meets the specification. The measured IIP_2 when injecting the receiver with a tone in Band 2 and measuring in Band 9 was 31.5 dBm. The IIP_2 performance of this receiver is very good, without the use of any calibration scheme due to the LNA frequency response.

The bandpass filter achieves approximately 7.5 dB rejection of the closest adjacent channel and greater than 12 dB rejection of the second adjacent channel. Since the LNA does not

have a flat frequency response, it also contributes to the adjacent channel rejection. The variation in the adjacent channel rejection over bands is due to the frequency response of the LNA. The total measured tuning range of the BPF was ± 300 MHz.

The measured image rejection of the receiver is shown in Fig. 21. The image rejection is determined by the load tuning of the LNA. In the lowest band, since the image is only 1584 MHz away, the image rejection is lowest. Image rejection increases to 36 dB as the center frequency of the band increases, since the image moves closer to DC. The overall image rejection will be significantly improved by the off-chip filter.

Power consumption of the receiver is shown in Table I and the receiver performance is summarized in Table II. The receiver consumes only 19.5 mA at a DC bias voltage of 2.3 V. Total active die area was 0.35 mm².

IX. CONCLUSION

This paper presented a receiver design for an MB-OFDM system that does not employ on-chip inductors. The new architecture presented in this paper realizes significant die savings, while maintaining adequate performance for a robust MB-OFDM system. Additionally, the design has an on-chip tunable bandpass filter and integrated input matching. Compared to a standard wideband receiver design, this architecture offers the advantage of smaller die area, simpler design, no external components and dynamic rejection of out-of-group jammers. The design is an attractive approach for a highly integrated UWB receiver in a standard CMOS process.

ACKNOWLEDGMENT

The authors wish to acknowledge the assistance and support of Qualcomm, the Center for Wireless Communication at UC San Diego, Dr. J. Foerster of Intel and Jazz Semiconductor for processing.

REFERENCES

- [1] A. Batra, J. Balakrishnan, R. Aiello, J. Foerster, and A. Dabak, "Design of a multiband OFDM system for realistic UWB channel environments," *IEEE Trans. Microw. Theory Tech.*, vol. 52, no. 9, pp. 2123–2138, Sep. 2004.
- [2] A. Ghosh, D. R. Walter, J. G. Andrews, and R. Chen, "Broadband wireless access with WiMAX/802.16: current performance benchmarks and future potential," *IEEE Commun. Mag.*, vol. 43, no. 2, pp. 129–136, Feb. 2005.

[3] M. Ranjan and L. Larson, "Distortion analysis of ultra wideband OFDM receivers," *IEEE Trans. Microw. Theory Tech.*, vol. 54, no. 12, pp. 4422–4431, Dec. 2006.

[4] —, "A sub-1 mm² dynamically tuned CMOS MB-OFDM 3-to-8 GHz UWB receiver front end," in *IEEE ISSCC Dig. Tech. Papers*, 2006, pp. 128–129.

[5] A. Ismail and A. Abidi, "A 3.1 to 8.2-GHz zero-IF receiver and direct frequency synthesizer in 0.18 μ m SiGe BiCMOS for mode-2 MB-OFDM UWB communication," *IEEE J. Solid-State Circuits*, vol. 40, no. 12, pp. 2573–2582, Dec. 2005.

[6] R. Roovers *et al.*, "An interference robust receiver for ultra-wideband radio in SiGe BiCMOS technology," *IEEE J. Solid-State Circuits*, vol. 40, no. 12, pp. 2522–2563, Dec. 2005.

[7] Y. Tsvividis, "Continuous-time filters in telecommunications chips," *IEEE Commun. Mag.*, vol. 39, no. 4, pp. 132–137, Apr. 2001.

[8] F. Sanders, B. Ramsey, and V. Lawrence, Broadband Spectrum Survey at Los Angeles, California, NTIA Report 97-336, 1997.

[9] V. Aparin and L. Larson, "Analysis and reduction of cross-modulation distortion in CDMA receivers," *IEEE Trans. Microw. Theory Tech.*, vol. 51, no. 12, pp. 1591–1602, May 2003.

[10] J. Lee and J. Cressler, "A 3–10 GHz SiGe resistive feedback low noise amplifier for UWB applications," in *Proc. IEEE Radio Frequency Integrated Circuits Symp.*, 2005, pp. 545–548.

[11] A. Ismail and A. Abidi, "A 3–10-GHz low-noise amplifier with wideband LC-ladder matching network," *IEEE J. Solid-State Circuits*, vol. 39, no. 12, pp. 2259–2268, Dec. 2004.

[12] A. Bevilacqua and A. Niknejad, "A ultrawideband CMOS low-noise amplifier for 3.1–10.6-GHz wireless receivers," *IEEE J. Solid-State Circuits*, vol. 39, no. 12, pp. 2269–2277, Dec. 2004.

[13] R. Gharpurey, "A broadband low-noise front-end amplifier for ultra wideband in 0.13- μ m CMOS," *IEEE J. Solid-State Circuits*, vol. 40, no. 9, pp. 1983–1986, Sep. 2005.

[14] K. H. Chen and C. K. Wang, "A 3.1 10.6 GHz CMOS cascaded two stage distributed amplifier for ultra-wideband application," in *Proc. IEEE Asia-Pacific Conf. Advanced System Integrated Circuits*, 2004, pp. 296–299.

[15] J. Hagen, *Radio Frequency Electronics*. Cambridge, U.K.: Cambridge Univ. Press, 1996.

[16] J. Yu and J. K. Fidler, "An automatic LC filter tuning system by optimization," in *Proc. 3rd IEEE Int. Conf. Electronics, Circuits and Systems*, 1996, pp. 215–218.

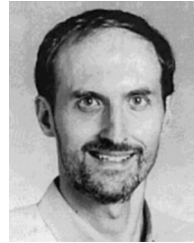
[17] W. B. Kuhn, "Fully integrated bandpass filters for wireless transceivers—problems and promises," in *Proc. 45th Midwest Symp. Circuits and Systems*, 2002, vol. 2, pp. 69–72.



cellular applications.

Mahim Ranjan (S'99–M'02) received the Bachelor degree in electrical engineering from the Indian Institute of Technology, Bombay, India, in 1999, and the Master and Ph.D. degrees in electrical and computer engineering from the University of California at San Diego in 2000 and 2006, respectively.

He was an Engineer with Magis Networks, San Diego, from 2001 to 2004, where he worked on RF transceivers for wireless multimedia. He currently works for Qualcomm Inc, San Diego, as a Senior Design Engineer, designing RF transceivers for



Lawrence E. Larson (S'82–M'86–SM'90–F'00) received the B.S. and M. Eng. degrees in electrical engineering from Cornell University, Ithaca, NY, in 1979 and 1980, respectively, and the Ph.D. degree in electrical engineering and the MBA degree from the University of California at Los Angeles (UCLA), in 1986 and 1996, respectively.

From 1980 to 1996, he was with Hughes Research Laboratories, Malibu, CA, where he directed the development of high-frequency microelectronics in GaAs, InP, and Si/SiGe and MEMS technologies.

In 1996, he joined the faculty of the University of California at San Diego (UCSD), La Jolla, where he is the Inaugural Holder of the Communications Industry Chair. He is currently Director of the UCSD Center for Wireless Communications. During the 2000–2001 academic years, he was on leave with IBM Research, San Diego, CA, where he directed the development of RF integrated circuits (RFICs) for third-generation (3G) applications. During the 2004 to 2005 academic year he was a Visiting Professor at TU Delft in the Netherlands. He has authored or coauthored over 250 papers and holds 31 U.S. patents.

Dr. Larson was the recipient of the 1995 Hughes Electronics Sector Patent Award for his work on RF MEMS technology. He was co-recipient of the 1996 Lawrence A. Hyland Patent Award of Hughes Electronics for his work on low-noise millimeter-wave high electron-mobility transistors (HEMTs), the 1999 IBM Microelectronics Excellence Award for his work in Si/SiGe HBT technology, and the 2003 IEEE Custom Integrated Circuits Conference Best Invited Paper Award.